

Utah State University

DigitalCommons@USU

Conference Proceedings

Materials Physics

6-25-2014

Electrostatic Discharge and Endurance Time Measurements of Spacecraft Materials: A Defect-Driven Dynamic Model

Allen Andersen

JR Dennison
Utah State University

Alec M. Sim
Utah State University

Charles Sim
Utah State University

Follow this and additional works at: https://digitalcommons.usu.edu/mp_conf

 Part of the [Condensed Matter Physics Commons](#)

Recommended Citation

Allen Andersen, JR Dennison, Alec M. Sim and Charles Sim, "Electrostatic Discharge and Endurance Time Measurements of Spacecraft Materials: A Defect-Driven Dynamic Model," Abstract 127, Proceedings of the 13th Spacecraft Charging Technology Conference, (Pasadena, CA, June 25-29, 2014), 11 pp..

This Conference Paper is brought to you for free and open access by the Materials Physics at DigitalCommons@USU. It has been accepted for inclusion in Conference Proceedings by an authorized administrator of DigitalCommons@USU. For more information, please contact digitalcommons@usu.edu.



Measurements of Endurance Time for Electrostatic Discharge of Spacecraft Materials: A Defect-Driven Dynamic Model

Allen Andersen, JR Dennison, Alec M. Sim, and Charles Sim

Abstract— Electrostatic breakdown leads to the majority of anomalies and failures attributed to spacecraft interactions with the plasma space environment. It is therefore critical to understand how electrostatic field strength (F_{ESD}) of spacecraft materials varies due to environmental conditions such as duration of applied electric field, rate of field change, history of exposure to high fields, and temperature. We have developed a dual-defect, thermodynamic, mean-field trapping model in terms of recoverable and irrecoverable defect modes to predict probabilities of breakdown. Fits to a variety of measurements of the dependence of F_{ESD} of insulating polymers on endurance time, voltage ramp rate, and temperature based on this model yield consistent results. Our experimental results for the prototypical materials low density polyethylene (LDPE) and polyimide (PI or Kapton HNTM) suggest that values of F_{ESD} from standard handbooks, or cursory measurements that have been used routinely in the past, substantially overestimate the field required for breakdown in common spacecraft applications, which often apply sub-critical fields for very long time periods as charge accumulates.

Index Terms— Electrostatic discharge, arcing, breakdown, spacecraft charging, space environment effects, polymers

I. NOMENCLATURE

| | |
|-------------------|--|
| a_{def} | = mean defect separation |
| D | = sample thickness |
| D_{bb} | = bond breaking dose |
| E_{strain} | = strain energy |
| F | = electrostatic field |
| F_{def}^s | = critical electrostatic field |
| F_{ESD}^s | = electrostatic breakdown field |
| $F_{ESD}^s(r_o)$ | = electrostatic breakdown field at 1 V/s ramp rate |
| F_{onset} | = onset electrostatic field for breakdown |
| h | = Planck's constant |
| I | = current |
| $K_{def}^{\pm s}$ | = rate of defect creation/annihilation (+/-) |
| k_B | = Boltzmann's constant |

| | |
|----------------------|---|
| N_{bond} | = density of carbon-carbon bonds |
| N_{def}^s | = defect density |
| N_{step} | = number of voltage steps to reach V_{static} |
| $n_{def}^s(t)$ | = time-dependent density of occupied defects |
| P_{def}^s | = probability of creating one defect |
| P_{step}^s | = probability of breakdown after N_{step} voltage increments |
| $P_{survive}$ | = probability to survive N_{step} voltage increments |
| P_{SVET} | = probability of breakdown for SVET test after $\Delta t_{elapsed}$ |
| q_e | = charge on electron |
| R_{lim} | = resistance of current limiting resistors |
| r | = voltage ramp rate |
| r_o | = voltage ramp rate of 1 V/s |
| T | = temperature |
| T_{melt} | = melting temperature |
| t | = time |
| t_{en} | = endurance time to breakdown |
| V | = applied voltage |
| V_i | = applied voltage at i^{th} step |
| V_{static} | = static applied voltage |
| Δt_{step} | = elapsed time during voltage increment |
| $\Delta t_{elapsed}$ | = elapsed time during ESD test |
| ΔF | = electrostatic discharge field distribution width |
| ΔG | = Gibbs activation energy |
| ΔG_{def}^s | = Gibbs defect activation energy |
| ΔV | = activation volume |
| ΔV_{def}^s | = defect activation volume |
| ΔV_{step} | = voltage change during voltage increment |
| Δt | = time interval field is applied |
| β | = Weibull function shape parameter |
| ϵ_o | = permittivity of free space |
| ϵ_r | = relative permittivity |
| v_{def}^s | = mean defect creation frequency |
| Ξ | = efficiency of radiation to break bonds |
| ρ_m | = mass density |

| s | Superscripts for defect type |
|-------|---|
| A | = type A irreversible defects |
| B | = type B reversible defects |
| bb | = broken bond defects |
| K | = Kuhn pair or kink defects |
| Tot | = total combined results for all defect types |
| S | = single type of defects |
| W | = estimate of defects by Weibull distribution fit |

Research was supported by funding from NASA Goddard Space Flight Center, a USU Blood Fellowship (Andersen), a Utah Space Grant Consortium Graduate Research Fellowship (A. Sim), a Utah State University Undergraduate Research and Creative Opportunities grant (C. Sim), and a Senior Research Fellowship from the Air Force Research Laboratory through the National Research Council. Allen Andersen, JR Dennison and Charles Sim are with the Materials Physics Group in the Physics Department at Utah State University in Logan, UT 84322 USA (e-mail: allen.andersen@aggiemail.usu.edu, JR.Dennison@usu.edu, charles.the.sim@gmail.com). Alec M. Sim is with the Department of Physical Sciences at Irvine Valley College in Irvine, CA 92618 USA (email: asim@ivc.edu).

II. INTRODUCTION

Electrostatic discharge (ESD) is the primary cause of space environment induced failures and anomalies [1]. As mission lifetimes and the sensitivity and complexity of instrumentation increase, so does the need for describing the influence of the electrical aging processes on ESD. This research studies the electrostatic field strength (F_{ESD}) of polymeric insulators as a function of applied field and the time-to-breakdown for applied fields less than F_{ESD} . A dynamic physics-based model for time-to-breakdown in terms of breakdown probabilities is much more valuable than an empirical static model, since it provides the ability to predict the statistical lifetime of dielectric materials subjected to prolonged stress from sub-critical electric fields. Insights into spacecraft failures follow from comparison of the field-dependent endurance times with times scales relevant to the space environment and orbital conditions [2].

We present experimental results for two prototypical polymeric materials, low density polyethylene (LDPE) and polyimide (PI or Kapton HNTM). F_{ESD} was determined using a custom high vacuum chamber, as a sustained rise in I-V curves. Ramp rates of ~ 6 V/s resulted in substantially lower F_{ESD} values than tests conducted with the maximum ramp rate of 500 V/s recommended in ASTM D3755 standards [3]. Time-dependent breakdown was studied with different tests, by applying a static field stress less than F_{ESD} across the material and measuring the endurance time. Taken together, these suggest that values of F_{ESD} from standard handbooks or cursory measurements that have been historically used by the spacecraft charging community can substantially overestimate F_{ESD} in common spacecraft situations.

These experimental results are compared with thermodynamic mean field multiple trapping models of the electric field aging process and with available prior measurements. We introduce a first-order approximation to develop an extended dynamic temperature-dependent electrostatic discharge model that include both reversible and irreversible defect mechanisms. Reversible defect mechanisms such as bond bending or twisting have energies less than or comparable to thermal energies, so that they can be readily repaired through thermal annealing. Irreversible defects such as bond stretching or breaking have higher energies. In the proposed mean field theory, each mechanism is characterized by a mean spatial separation of sites and a mean activation energy. The model predicts the observed measurements, which show a negative logarithmic decay of endurance time to electrostatic breakdown field. This is consistent with thermodynamic models, with F_{ESD} asymptotically approaching a constant value as the time-to-breakdown goes to infinity.

We also discuss these ESD results in terms of a more comprehensive unified theory for electron transport in highly disordered insulating materials, which allows a correlation between fitting parameters and more fundamental materials properties such as atomic scale structure and bonding, mobility, transition probabilities, and spatial and energetic distributions of trap states beyond the energy mean field approximation.

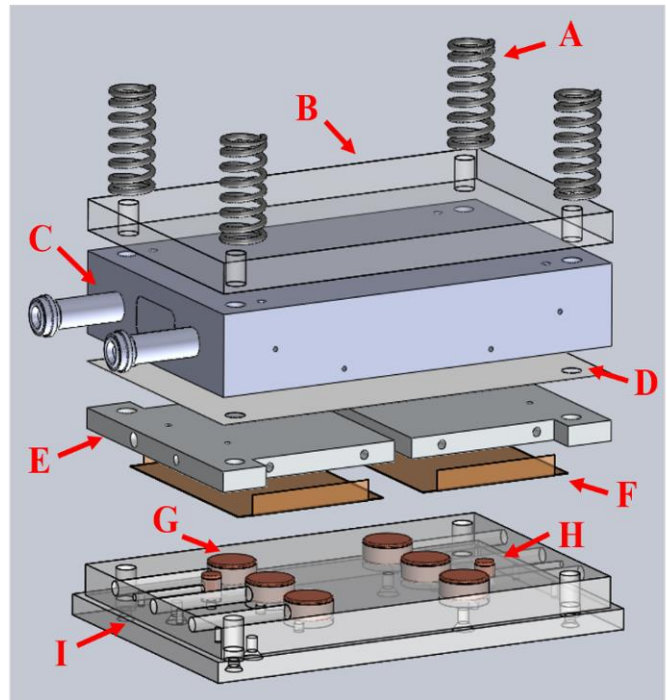


Fig. 1. Exploded view of ESD test assembly showing: (A) Adjustable pressure springs, (B) Polycarbonate insulating layer in cryogenic configuration—located between D and E during room temperature tests, (C) Cryogen reservoir, (D) Thermally conductive, electrically isolating layer, (E) Sample and mounting plate, (F) Sample, (G) HV Cu electrode, (H) Cu thermocouple electrode, (I) Polycarbonate base.

III. EXPERIMENTAL METHODS

Electrostatic discharge (ESD) tests were conducted using a modified ASTM method [4,5] in a custom, high vacuum chamber ($<10^{-3}$ Pa base pressure) [6]. Electric fields were applied to the material using a variable high voltage power supply (CPS Precision, Model 130N/1314; 0-30 kV $\pm <2\%$ at 5 mA) in a simple parallel plate capacitor geometry (Figs. 1 and 2). Voltage, V , and current, I , were monitored for the duration of the experiments using two interfaced multimeters (Amprobe®, Model 38XR-A; 100 μ V and 100 nA resolution at 2 Hz acquisition rate) under LabVIEWTM control.

Samples (F, in Fig. 1) were clamped between a metal sample mounting plate (E) and six highly polished (<200 nm rms surface roughness) Cu high voltage electrodes (G). This allowed testing of six samples during a single vacuum cycle. A spring clamping mechanism (A) was employed to apply uniform sample contact pressure of ~ 0.4 MPa, in compliance with standard methods [4].

Three types of ESD measurements were made: dynamic incremental-voltage breakdown (step-up) tests (see Fig. 4(a)), static voltage endurance time (SVET) tests (see Fig. 4(b)), and temperature-dependent step-up measurements. All three types of measurements began by incrementing the applied voltage at $V_{step} \approx 20$ V at $\Delta t_{step} \approx 3.5$ s time intervals (more precisely, on a cycle of three 16 ± 1 V increments at 3.00 ± 0.02 s intervals followed by one 33 ± 1 V increment at a 4.00 ± 0.02 s time interval) up to 30 kV (blue regions in Fig. 3). For step-up tests (see Fig. 3(a)), the voltage was increased incrementally at constant rate until complete breakdown occurred. For step-up

measurements, current increased significantly at breakdown (typically up to on the order of 10 μA) and continued to rise linearly above breakdown, with a slope set by the sum of the residual sample resistance and two in series current limiting resistors ($R_{Lim}=100\text{ M}\Omega$ in Fig. 2).

Static voltage endurance time (SVET) measurements of the endurance time, t_{en} , of electrostatic breakdown (see Fig. 3(b)) were conducted by similarly incrementing the applied voltage to a plateau voltage, V_{static} , and then maintaining this static electric field across the sample until complete electrostatic breakdown occurred. Typical static voltages for the endurance time experiments described here were in the range of 4 kV to 9 kV. These values yielded endurance times from a few minutes to a few days. The appropriate value of the endurance time, as determined from the elapsed time as logged by the data acquisition program measured from when the initial voltage was applied, is discussed in Section V.B.

Temperature-dependent measurements were conducted over a range from $\sim 150\text{ K}$ to 325 K . Measurements were made by cooling samples in thermal contact with an aluminum liquid nitrogen filled cryogen reservoir (C). Temperature was monitored with Type K thermocouples attached to two Cu temperature sensors (H) in good thermal contact with the sample, but electrically isolated (I). Temperatures typically increased less than 0.6 K/min or $\lesssim 15\text{ K}$ during a single cryogenic step-up testing cycle.

Samples of branched LDPE used in studies described here ([3,7], ASTM D-5213 type I) of $29.7\pm 2\%$ μm average measured thickness ($\lesssim 2\%$ average thickness variation for any one sample) had a density of $0.92\pm 0.01\text{ g/cm}^3$ [7] with an estimated crystallinity of 50% [8], an estimated peak fractional mass distribution of $\sim 6\cdot 10^3\text{ amu}$ or $\sim 2\cdot 10^3\text{ C}_2\text{H}_4$ mers per chain [6,9], and a relative dielectric constant of 2.26 [7]. Samples of Kapton HNTM ([3,10], ASTM D-5213 type I) of $23.9\pm 4\%$ μm average measured thickness (3% average thickness variation for any one sample) had a density of $1.43\pm 0.01\text{ g/cm}^3$ [10], and a relative dielectric constant of 3.5 [10]. A single mer of Kapton HNTM has an atomic composition of $\text{C}_{22}\text{O}_5\text{N}_2\text{H}_{10}$ [10].

All samples were chemically cleaned with methanol prior to a bakeout at $338\pm 1\text{ K}$ under $\sim 10^{-3}\text{ Pa}$ vacuum for $>24\text{ hr.}$ while in contact with a grounded surface to eliminate absorbed water and volatile contaminants and any residual stored charge; samples conditioned in this manner had a measured outgassing rate of $<0.05\%$ mass loss/day at the end of bakeout, as determined with a modified [6,11] ASTM 1559 [12] test procedure.

IV. THEORY

Electrical aging or stress (prolonged exposure to high electric fields) can cause breakdown in insulating materials. Aging in the spacecraft environment is induced by high energy particle flux into or through a material, by medium to high applied electric fields, or by contact carrier injection [2]. Numerous studies have shown that electrical aging can be characterized by (i) the density of defects created within the material from bond stress due to local and applied electric fields and (ii) the Gibbs free energy, bond destruction energy, or cohesion energy associated with creation of these defects

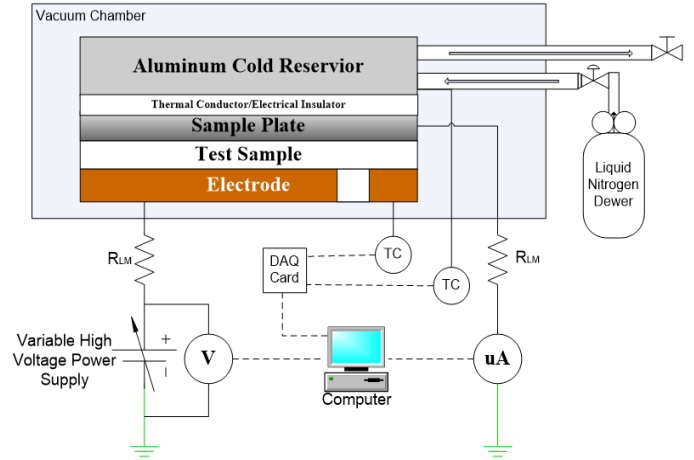


Fig. 2. Block diagram of ESD test apparatus. Shown are a simple parallel plate capacitor sample geometry with high voltage power supply, a cryogenic reservoir in thermal contact with sample plate, plus computer-automated voltage, current and temperature sensors.

[13-17].

A. General Breakdown Theory

To understanding how the bonds within a polymeric material are affected by an applied stress due to internal or external electrostatic fields, consider an electric field F across two faces of a cubic unit volume acting as a parallel plate capacitor. The strain energy required to compress this unit volume by an amount ΔV is [18]

$$E_{strain} = \frac{1}{2}\epsilon_0\epsilon_r F^2 \Delta V. \quad (1)$$

More detailed vector or tensor calculations of the strain energy for more realistic, anisotropic shapes yield similar results that differ only by a constant of order unity. Alternate theories [8,12,14-17], which produce equivalent results, consider the energy, $q_e a F$, acquired by a charge carrier with charge q_e as it moves through a mean field, F , over a mean separation distance between defects, a ; to account for the dielectric response of the material, the carrier charge density is replaced with $(q_e/a^2) = \frac{1}{2}(\epsilon_0\epsilon_r F)$.

Now consider a density of defects—*e.g.*, ionization sites or broken bonds—associated with electrostatic discharge, N_{def} , and a cubic mean activation volume, $\Delta V_{def} = (a_{def})^3 \equiv 1/N_{def}$, associated with one such defect. For comparison, in LDPE the approximate density of C_2H_4 mers is $\sim 2\cdot 10^{22}\text{ cm}^{-3}$, polymer chains is $\sim 8\cdot 10^{18}\text{ cm}^{-3}$, and crystalline lamella is $\sim 10^{15}\text{ cm}^{-3}$ based on measured physical properties of the material. If we set the strain energy of Eq. (1) in a volume ΔV_{def} equal to the Gibbs defect activation energy ΔG_{def} , we can solve for the critical electric field, F_{def} , just strong enough to produce one defect per activation volume:

$$F_{def} = \left[(2/\epsilon_0\epsilon_r) N_{def} \Delta G_{def} \right]^{1/2}. \quad (2)$$

For permanent defects, the critical field represents a mean electrostatic field energy density large enough that on average defects are generated in every activation volume and breakdown is complete. At fields somewhat below the critical field, one can envisage interconnected regions of defective

activation volumes—that have essentially undergone an insulator-to-conductor transition—that allow current to propagate through the material via a percolation-like network. Such a percolation-like model lends itself to a decrease in (but still finite) probability of breakdown with decreasing field—as the probability of completing a percolation path across the sample at a given defect density decreases; this also predicts an onset field, F_{onset} , at the percolation threshold for defect densities below which breakdown will not occur. For processes that permit repair of the defect, dynamic percolation models need to incorporate defect activation volumes with a finite lifetime. Estimates of the defect activation energies and defect densities for the samples studied here, and the associated critical and onset fields, are presented in Section IV.C where they are compared with measured results.

B. Endurance Time Equation

Given a model for the critical field, a thermodynamic model for the electric field aging process has been developed to predict the mean time to failure or endurance time, t_{en} , as a function of high electric field and temperature [15,17,19-21]. There are direct equivalences between the thermodynamic model for ESD and Mott's model for thermally activated hopping conductivity [22]. As with this conductivity model, ΔV_{def} and ΔG_{def} represent a mean defect activation volume (or barrier width) and a mean defect activation energy (or barrier height of the energy well), respectively (see Fig. 4(a)) [8,23].

On average the forward and backward movements of charge carriers from one trap state to an adjacent site can be thought of as a rate process, where motion with (against) the field decreases (increases) the barrier height of the Gibbs free energy, as shown in Fig. 4(b). At breakdown, the critical energy gained from electron motion through the electric field across a defect volume of width a_{def} from Eq. (1), is just sufficient to overcome the barrier height ΔG_{def} . This results in the hyperbolic sine function in Eq. (3) for the probability of breakdown as a function of applied field F , temperature T , and time the field is applied Δt [20]:

$$P_{def}(\Delta t, F, T) = \left(\frac{2k_B T}{h / \Delta t} \right) \exp \left[\frac{-\Delta G_{def}}{k_B T} \right] \sinh \left[\frac{\epsilon_0 \epsilon_r F^2}{2k_B T N_{def}} \right]. \quad (3)$$

The development of Eq. (3) is reminiscent of the early hopping conductivity work of Miller and Abrahams [24].

The probability to create one defect per unit volume ΔV_{def} is equal to unity at the endurance time, $P_{def}(\Delta t=t_{en})=1$. (P_{def}/t_{en}) corresponds to the mean defect creation frequency, ν_{def} ; thus, $h\nu_{def}=h/t_{en}$ can be thought of as the quantum energy uncertainty for a broken bond or P_{def} as the probability of tunneling through the barrier in Fig. 4. Solving Eq. (3) with $P_{def}=1$ for the endurance time to breakdown under an applied field, we find

$$t_{end}(F, T) = \left(\frac{h}{2k_B T} \right) \exp \left[\frac{\Delta G_{def}(F, T)}{k_B T} \right] \operatorname{csch} \left[\frac{\epsilon_0 \epsilon_r F^2}{2k_B T N_{def}(F, T)} \right]. \quad (4)$$

The defect activation energy ΔG_{def} and the number density of defects N_{def} , are the field- and temperature-dependent fitting

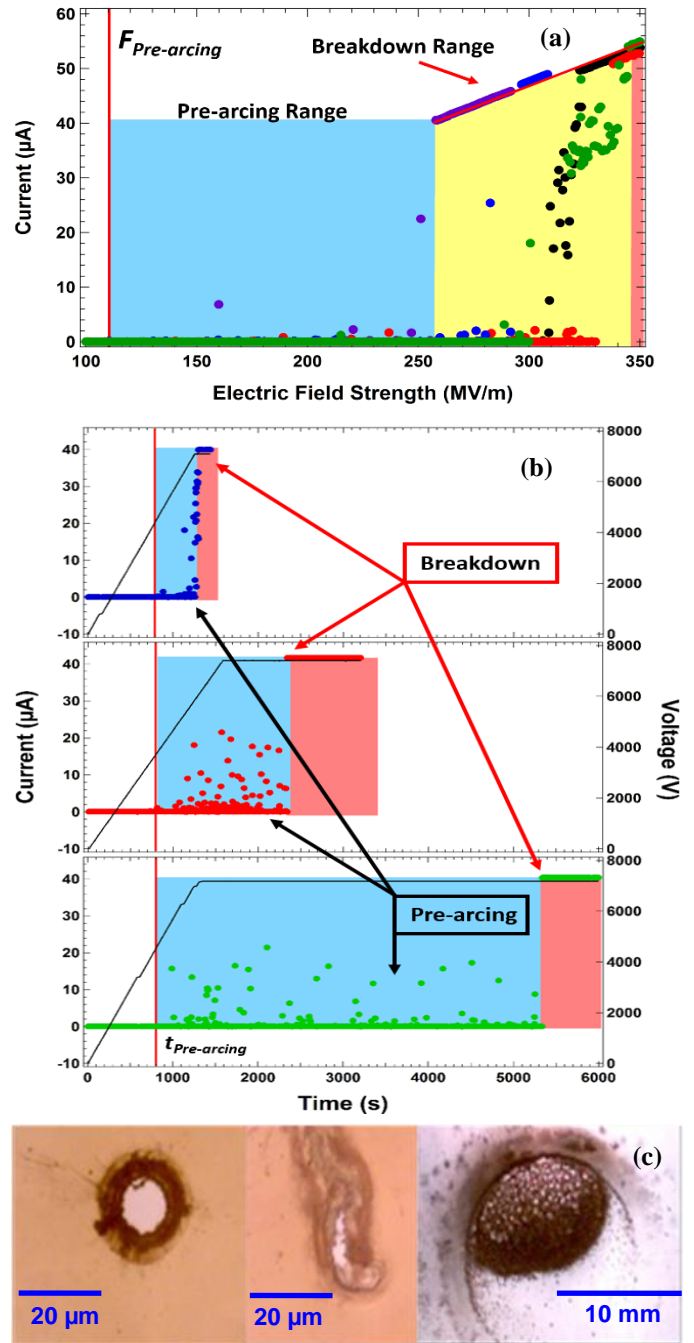


Fig. 3. Evidence of electrostatic breakdown. (a) Plot of five step-up tests of LDPE. The pre-breakdown region is highlighted in blue, the complete breakdown region in red, and the intermediate region in yellow. (b) Comparison of three endurance time breakdown tests at static applied fields of 280 MV/m, 247 MV/m and 243 MV/m (from top to bottom). Tests reached the static voltage at 1400 ± 170 s; black lines referenced to vertical axes on the right show the voltage versus time profiles. Complete breakdown occurs at t_{en} where the IV curves increase to a constant value of ~ 40 nA set by the current limiting resistors. (c) Images of breakdowns damage sites: the thermoset polymer Kapton E (left) usually breaks down with circular holes, while the thermal plastic LDPE (center) is more irregular. Expanded PTFE (right) can breakdown rather spectacularly due to large amounts of charge stored in the high density of mechanical voids in the material. Note the much larger length scale for the expanded PTFE damage site.

parameters of the model. ϵ_r is the relative dielectric constant and a property of the material. Planck's constant h , the Boltzmann constant k_B , and the permittivity of free space ϵ_0 are fundamental physical constants. The applied field F and

temperature T are independent variables that can be changed with each measurement.

Alternately, one can consider material breakdown as a function of the number of *occupied* defects, $n_{def}(t)$. The rate of net defect creation is equal to the difference of two terms—the first for defect creation and the second for defect repair—each of which is the product of the number of sites for defect formation (or annihilation) times a defect creation (or annihilation) rate function:

$$\frac{dn_{def}(t)}{dt} = [N_{def} - n_{def}(t)] \cdot K_{def}^+(F, T) - n_{def}(t) \cdot K_{def}^-(F, T). \quad (5)$$

This model [25], based on rate theory and the idea that the defect creation or bond breaking kinetics should be similar to kinetic rate reactions in chemical systems, provides a way to calculate the increase in defect density as a function of time and temperature. An expression for the rate at which defect creation (K_{def}^+) and annihilation (K_{def}^-) occurs is

$$K_{def}^{\pm}(F, T, t) = \frac{k_B T}{h} \exp\left[-\frac{\Delta G_{def}^i \pm \frac{1}{2} F(t)^2 \epsilon_o \epsilon_r \Delta V_{def}^i}{k_B T}\right] \quad (6)$$

$$= \frac{k_B T}{h} \exp\left[\left(F(t)^2 \pm F_{critical}^2\right) \frac{\epsilon_o \epsilon_r}{2 N_{def}(F, T) k_B T}\right]$$

using Eq. (2) and the relation $\Delta V_{def} = I/N_{def}$. Note Eq. (6) follows directly by equating K_{def}^{\pm} to the time derivative of Eq. (3). Here, \pm refers to motion of negative charge carriers with or against the field. Also note that the rate functions, K_{def}^{\pm} , can be—and usually are—functions of both applied field and temperature. They can also be time dependent through a time-dependent component of the internal electric field from the accumulation of charge within the material or a time-dependent defect density, $N_{def}(t)$.

Using Eqs. (5) and (6), one can recover the results in Eq. (3) and show that $P_{def}(t) \propto \Delta t [dn_{def}(t)/dt]^{-1}$. Equation (5) suggests an important connection between the rate of bond breaking and resulting creation of electron traps. In particular, it can be shown using a multiple trapping transport theory [26] that the solution to Eq. (5) for the number of bonds broken as a function of time, temperature and applied field is consistent with impact ionization rate equation models proposed by Kao [13]. This connection suggests that for studies using the configuration shown in Fig. 2, but for applied fields normally considered safe, many materials will fail after very long exposure to intermediate fields. This behavior has been observed in many polymers and other highly disordered insulating materials.

Trnka [27] discusses the basic Crine model [15,19] that we extend and emphasizes the importance of improvements to endurance theory coupled with accelerated laboratory testing. Czaszejko [28], Griffiths [21], Dang [29], and Dissado and Fothergill [17] review alternate theories relating the endurance time to the electrostatic breakdown and temperature, such as the more simple inverse power law model [17] and the more

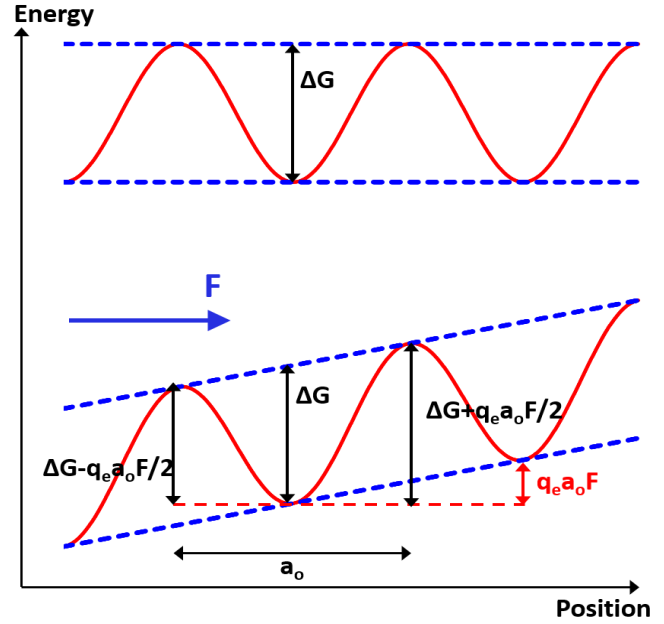


Fig. 4. Potential energy versus position with (top) no electric field and (bottom) electric field. The field stress acts to reduce the energy necessary to initiate the degradation process through thermally assisted tunneling from the defect energy (Gibbs energy of activation, ΔG_{def}) by an amount $\frac{1}{2} q_e a_{def} F_{def}$, where a_{def} is the mean defect separation. The red curves are the carrier potential and the blue dashed curves are the field energy, as functions of position.

complete electrokinetic endurance model [29,30] that predicts a threshold value for electrostatic breakdown at long endurance times. All these theories predict roughly similar values for endurance and approximately similar temperature dependence in the range of endurance times typically measured by experimental tests, that is, in the range of 10^0 to 10^6 s [29].

C. Defect Mechanisms

We turn our attention now to specific processes involved in ESD to establish relevant values for N_{def} and ΔG_{def} . Consider two types of breakdown processes, Types A and B, as illustrated in Figs. 5(a) and 5(b), respectively. Type A processes are lower energy *reversible* process, that have a significant rate of defect repair. Type B processes are higher energy largely *irreversible* processes, with a negligible defect repair rate, at relevant temperatures.

In Type B viscous or inelastic deformation processes, breakdown of the material is due to direct stress on molecular segments causing irreparable damage with no bond repair possible [31], where the ends of broken bonds with unpaired sites can act as electron traps [13,19,30]. In these processes, there is little ionization or segmental motion. Such defects can be generated by the breaking of carbon-carbon bonds of the C_2H_4 monomer alkane single bonds along polymer chains, with dissociation energy $\Delta G_{def}^{bb} = 3.65$ eV/bond [32]. We can expect similar values of ΔG_{def}^{bb} for many polymers, due to the similarity in carbon-carbon bonds in their polymer chains. The energy distribution for the deep level defects should be fairly narrow since the bonds are relatively homogeneous. ΔG_{def}^{bb} will be largely independent of the environment surrounding the bond and should not depend on the orientation

of the bond with respect to the field since it is an impact ionization process creating a point defect. The bond breaking process will not have a significant temperature dependence at accessible temperatures below the melting temperature T_{melt} or decomposition temperature, since $k_B T < k_B T_{melt} \ll \Delta G_{def}^{bb}$; hence K_{def}^{+B} will not be temperature or field dependent and K_{def}^{-B} will be negligible.

The total density of such bonds can be estimated from the mass density of LDPE and the mass of the mer (assuming one bond per mer) to be $N_{bond} \lesssim 4 \cdot 10^{22}$ bonds/cm³. The density of broken bonds at complete breakdown can be estimated from radiation damage studies as $N_{def}^{bb} \lesssim [\frac{1}{2} D_{bb} \rho_m \bar{\epsilon} / \Delta G_{def}^{bb}] \approx 1.5 \cdot 10^{18}$ broken bonds/cm³, where: (i) the dose (deposited energy—from the field or from incident electron radiation—per unit mass) at breakdown $D_{bb} \sim 2 \cdot 10^5$ Gy, since irrecoverable electron radiation damage (e.g., electron transport and emission properties) typically occurs for doses $\geq 10^5$ Gy [33,34] and mechanical failure occurs at $\geq 10^6$ Gy [35]; (ii) from radiation damage experiments, the mean energy required to break such a bond is $[\Delta G_{def}^{bb} / \bar{\epsilon}] \approx 130$ eV [36]; and (iii) the efficiency of radiation to break bonds, $\bar{\epsilon} \approx 36$ [36]. This independent estimate of broken bonds in the amorphous region $\lesssim [D_{bb} \rho_m \bar{\epsilon} / \Delta G_{def}^{bb}] \approx 7.5 \cdot 10^{18}$ broken bonds/cm³ is consistent to the estimated density of chains, $\sim 1.5 \cdot 10^{18}$ broken bonds/cm³ (see Section IV.A), since there is one broken bond per chain. Note, both N_{bond} and N_{def}^{bb} should be reduced by $\sim 1/2$, since ESD is limited to transport across amorphous regions and N_{def}^{bb} is further reduced by a factor of $1/3$ when a percolation threshold in the amorphous region is taken into account [37]. The value obtained, $N_{def}^{bb} \approx 1.5 \cdot 10^{18}$ cm⁻³, is consistent with a range of published values for LDPE near $1-3 \cdot 10^{18}$ cm⁻³ [6,38]. Since $N_{bond} \gg N_{def}^{bb} > n_{def}^{bb}(t)$, $n_{def}^{bb}(t)$ is negligible in the first term of Eq. (5). Taken together, these estimates, in conjunction with Eq. (2), lead to a critical field for broken bond defects of $F_{def}^{bb} \sim 295$ MV/m, with $N_{def}^{bb} \approx 1.5 \cdot 10^{18}$ broken bonds/cm³ and $\Delta G_{def}^{bb} = 3.65$ eV/bond.

Type A processes are reversible; that is, they require a low enough activation energy that such defects can be spontaneously repaired due to thermal activation. These can include weak van der Waals bonds and main chain reconfiguration energies such as chain rotations and kinks. Creation of such defects in molecular or crystalline segments of the polymer chains result either from charge injection and impact ionization or from conformational defect (kink) generation [13]. As the injected charge becomes trapped at these defect sites in the ionized molecular segments and on chain segments, a high localized field develops leading to breakdown.

We consider one potential type of reversible defects further, kink defects. *Trans-gauche* rotational barriers for typical isolated longer alkane chains are 0.36 eV/kink. In polymers, close proximity of other chains leads to chain-chain interactions and steric hindrance that limits kink formation. It is often found that formation of two kinks in close proximity (which minimize displacement of the overall chain) are energetically more favorable than formation of a single kink

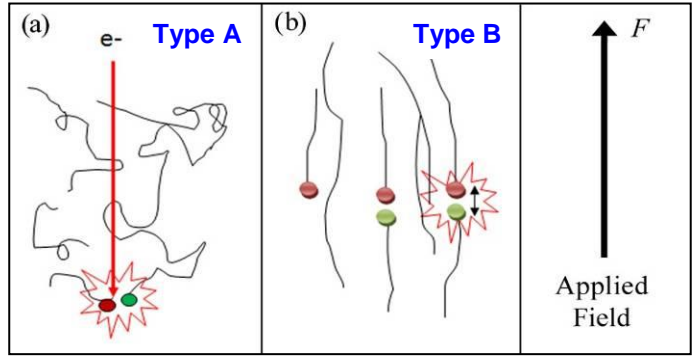


Fig. 5. Typical electrostatic breakdown mechanisms. (a) Type A low energy, reversible breakdown mechanisms due to creation of recoverable defects caused, for example, by charge injection, impact ionization, or kink formation. (b) Type B high energy, irreversible breakdown mechanisms due, for example, to chain bond breaking from direct stress causing irreparable damage.

and the concomitant large displacement of the rest of the chain. This is referred to as formation of a Kuhn pair, with a minimum kink separation (Kuhn length) of ~ 3.5 C-C bond lengths (~ 1.3 nm) for LDPE [18]. A very crude estimate of the magnitude of this effect is based on the $\sim 25\%$ increase in maximum working temperatures of cross-linked polyethylene over low density polyethylene. We can therefore estimate the defect energy as approximately twice the kink formation energy plus $\sim 25\%$ additional energy to account for chain-chain interactions and steric hindrance; $\Delta G_{def}^K = (1.25 \cdot 2 \cdot 0.36$ eV/kink) = 0.90 eV. An upper bound on N_{def}^K can be estimated as $\sim 14\%$ of the mer density (see Section IV.A), $N_{def}^K < 3 \cdot 10^{21}$ Kuhn pairs/cm³; this assumes a minimum separation of Kuhn pairs equal to the minimum kink separation of 3.5 mers and that only $\sim 50\%$ of the total chains can contribute, since only chains in the amorphous region are free to develop kinks unhindered. Using these same approximations for polyimide, with a working temperature $\sim 75\%$ above LDPE [10], minimal crystallinity, and a Kuhn length of ~ 8 nm [39], predicts $\Delta G_{def}^K = 1.3$ eV and $N_{def}^K < 5 \cdot 10^{20}$ Kuhn pairs/cm³.

We can expect that ΔG_{def}^K will be substantially different for different polymers, due to strong variations in the chain structure, rigidity and crosslinking. The energy distribution for these defects should be broader, since the local chain environments are not homogeneous. ΔG_{def}^K should depend on the orientation of the bond with respect to the field, since this provides the torque to reorient the chains. The applied field has a well-defined direction; however the field due to internal charge accumulation will be largely isotropic and will not provide net torque. There may even be a saturation effect, as more kinks develop to align the chain segments in the disordered regions with F or as bond breaking becomes prevalent producing shorter chains which align more easily with the field. The kink formation process will also have a significant temperature dependence at accessible temperatures below the melting temperature or decomposition temperature. Thermal annealing may also act to reduce the equilibrium defect density for these lower energy defects. Hence K_{def}^{+A} will be both temperature and field dependent and K_{def}^{-A} will not be negligible.

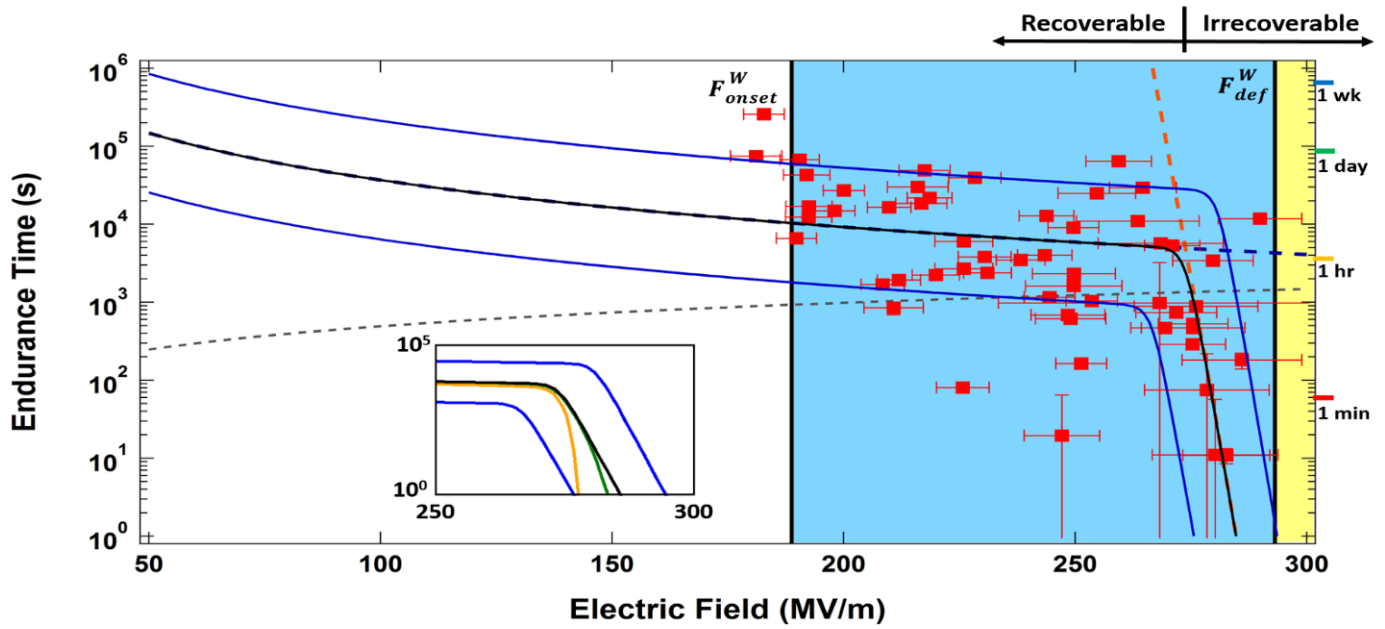


Figure 6. Dual mechanism multiple trapping model fit against endurance time data for LDPE, with $F_{def}^W=293$ MV/m, $F_{onset}^W=189$ MV/m. Data are fit (black line) with the dual-defect extension of the Crine model [15,19,27] given by Eq. (8), with $\Delta G_{def}^A=0.95$ eV, $\Delta G_{def}^B=3.65$ eV, $N_{def}^A=7\cdot 10^{21}$ cm⁻³, and $N_{def}^B=1.75\cdot 10^{18}$ cm⁻³. The blue lines show fits with $\pm 5\%$ variations in the ΔG_{def}^A and ΔG_{def}^B fitting parameters. The dashed lines indicate the separate contributions from Type A (blue) and Type B (orange) defects. The colored bars on the right axis indicate the time scales in larger units. The grey dotted line shows the ramping time to a given field for the data acquired at 20 V per 3.5 s. The inset shows the influence of the ramping process on the measured time to breakdown: the black curve assumes no contribution from the ramping process, the yellow curve assumes each ramp step field places as much stress on the material as the static field, and the green curve weights each ramp time interval with the appropriate field dependent failure probability from Eq. (7). Note that even at high fields the discrepancy between the correct (green) curve and the approximate (black) curve is $< 5\%$ at $t_{en} \geq 1$ s and is $< 20\%$ of the variation due to $\pm 5\%$ uncertainties in the defect energies at $t_{en}=1$ s. Error bars in time for the data are less than the size of the symbols, except as shown at $t_{en} < 200$ s. Error bars in electric field are largely determined by the $\sim 2\%$ variations in film thickness.

V. ELECTROSTATIC BREAKDOWN MEASUREMENTS

A. Dual Mechanism Model Fit to Data

Figure 6 shows the measured data for time to breakdown as a function of applied field for LDPE endurance time tests for the data acquired at 20 V per 3.5 s ramp rate to a static voltage. There are data from 55 step-up tests shown, which took a total of 272 hr acquisition time. Measured endurance times conducted at electric fields from 180 to 290 MV/m spanned almost five orders of magnitude in time from ~ 10 s to several days. The colored bars on the right axis indicate the time scales in larger units. Error bars in time for the data are less than the size of the symbols, except as shown at $t_{en} < 200$ s. Error bars in electric field are largely determined by the $\sim 2\%$ variations in film thickness.

There is a definite transition between two separate field regimes evident in Fig. 6, suggesting that a new composite model is required which incorporates at least two defect mechanisms. The data below ~ 270 MV/m with endurance times on the order of a few hours to several days were dominated by the recoverable processes and can be fit (blue dashed curve) by Eq. (4) with $\Delta G_{def}^A=0.95$ eV and $N_{def}^A=7\cdot 10^{21}$ cm⁻³. The data above ~ 270 MV/m with endurance times on the order of ~ 10 s to ~ 1 hr. can also be fit (red dashed curve) separately by Eq. (4) with $\Delta G_{def}^B=3.65$ eV and $N_{def}^B=1.5\cdot 10^{18}$ cm⁻³. The dual mechanism multiple trapping model (black line Fig. 6) equates the total probability of failure from either type of defect to the sum of failures for both Type A and Type B processes:

$$P_{def}^{Tot}(\Delta t, F, T) = \sum_{i=A,B} P_{def}^i \quad (7)$$

$$= \left(\frac{2k_B T}{h / \Delta t} \right) \sum_{i=A,B} \exp \left[\frac{-\Delta G_{def}^i}{k_B T} \right] \sinh \left[\frac{\epsilon_o \epsilon_r F^2}{2 N_{def}^i k_B T} \right].$$

This assumes the probabilities P_{def}^A and P_{def}^B are independent of the other defect type. Once again, to find t_{en} , we set $P_{def}^{Tot}=1$ in Eq. (7) and solve for $t_{en}=\Delta t$. Thus,

$$t_{en}(F, T) = \left(\frac{h}{2k_B T} \right) \left\{ \sum_{i=A,B} \exp \left[\frac{-\Delta G_{def}^i}{k_B T} \right] \sinh \left[\frac{\epsilon_o \epsilon_r F^2}{2 N_{def}^i k_B T} \right] \right\}^{-1}. \quad (8)$$

The values for the fitting parameters are in excellent agreement with the values predicted in Section IV.C. For Type B irreparable defects, ΔG_{def}^B and N_{def}^B agree with the predicted values $N_{def}^{bb} \approx 1.5\cdot 10^{18}$ broken bonds/cm³ and $\Delta G_{def}^{bb}=3.65$ eV/bond. For Type A repairable defects, ΔG_{def}^A and N_{def}^A agree with the predicted values $N_{def}^K \approx 3\cdot 10^{20}$ Kuhn pairs/cm³ and $\Delta G_{def}^K=0.90$ eV. Errors in the fitting parameters are estimated by assuming a $\pm 5\%$ deviation in the values of ΔG_{def}^A and ΔG_{def}^B used in Eq. (8) to produce the blue curves in Fig. 6; these show a maximum deviation in the endurance time of ~ 1 order of magnitude consistent with a spread in the measured data.

B. Correction for Ramping Time

Note that the endurance time used to generate the black curve in Fig. 6 is approximated as the elapsed time at the static field, and does not include the ramping (step-up) time. At short elapsed times this overestimates the endurance time. However, this is significant only for endurance times comparable to or less than ramp times of ~20 min, where the dotted line in Fig. 6 showing ramping time to a given field for the data acquired at 20 V per 3.5 s crosses the endurance curve. The inset in Fig. 6 shows the influence of the ramping process on the measured time to breakdown: the black curve assumes no contribution from the ramping process, the yellow curve assumes each ramp step field places as much stress on the material as the static field, and the green curve weights each ramp time interval with the appropriate field dependent failure probability (see Eq. (12) derived below). Note that even at high fields, the discrepancy in F_{ESD} between the correct (green) curve and the approximate (black) curve is <5% at $t_{en} \geq 1$ s and is <20% of the variation due to $\pm 5\%$ uncertainties in the defect energies at $t_{en} = 1$ s. Error bars in time for the data are less than the size of the symbols, except as shown at $t_{en} < 200$ s.

We now develop the correction for ramping time from probability considerations. The probability to break down when exposed to a field F for a time Δt is given by Eq. (3) or Eq. (7); the probability of survival is $[1 - P_{Tot}(\Delta t, F, T)]$. The probability to survive N_{step} incremental voltage steps of ΔV_{step} volts, each for a time Δt_{step} , up to a static voltage $V_{static} = N_{step} \Delta V_{step}$ is the product of the survival probabilities of each increment:

$$P_{Survive}^{Tot}(\Delta t_{step}, N_{step}, \Delta V_{step}, T) = \prod_{j=1}^{N_{step}} \left[1 - P_{def}^{Tot} \left(\Delta t_{step}, \frac{j \Delta V_{step}}{D}, T \right) \right]. \quad (9)$$

The complementary probability of breakdown, $P_{step} = (1 - P_{Survive})$, is

$$P_{step}^{Tot}(\Delta t_{step}, N_{step}, \Delta V_{step}, T) = 1 - \prod_{j=1}^{N_{step}} \left[1 - P_{def}^{Tot} \left(\Delta t_{step}, \frac{j \Delta V_{step}}{D}, T \right) \right]. \quad (10)$$

Figure 7 shows P_{step}^{Tot} for step-up tests as a function of applied field up to a maximum field of 250 MV/m for four different ramp rates, including the 20 V steps at 3.5 sec intervals used most often in the tests reported here and for a maximum ramp rate of 500 V/s intervals as recommended in the ASTM standard [5]. As expected, the probability of breakdown decreases for faster ramp rates. The analysis in Fig. 7 uses Eq. (10) with $\Delta G_{def}^A = 0.95$ eV and $N_{def}^A = 2.8 \cdot 10^{21}$ cm⁻³, and $\Delta G_{def}^B = 1.07$ eV and $N_{def}^B = 3.15 \cdot 10^{19}$ cm⁻³ (see Section III.D). Depending on the material and the application it can often be a reasonable approximation to ignore the contribution from Type A defects since the endurance times found for Type A separately are long compared to the ramp times for the data in Fig. 6 (compare the red dashed curve with the block dotted curve).

Finally, the probability of breakdown occurring in a SVET test over an elapsed time $\Delta t_{elapsed} > N_{step} \Delta t_{step}$ due to either a

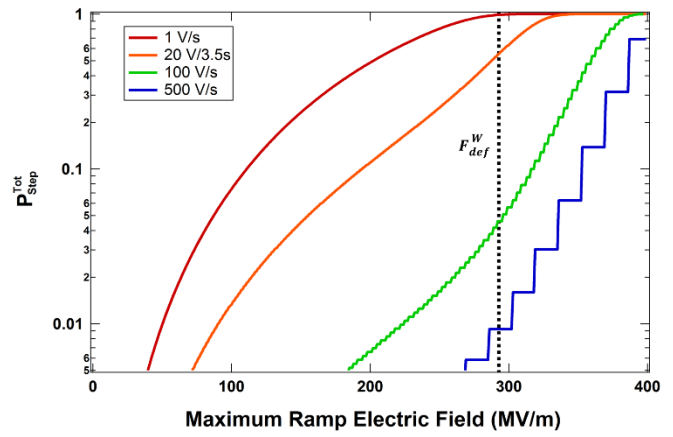


Fig. 7. Cumulative probability of breakdown during the voltage step-up process as a function of ramp maximum electric field. Results shown are based on Eq. (10) using values from the P_{step}^{Tot} fit used in Fig. 9 (a) for four ramp rates up, including the typical experimental ramp rate of 20 V per 3.5 s and the ASTM upper bound of ramp rates, 500 V/s. The vertical dashed line indicates the experimental value of F_{def}^W at 20 V per 3.5 s, 293 MV/m.

breakdown during ramping or at V_{static} is the sum of Eqs. (7) and (10):

$$P_{SVET}^{Tot}(\Delta t_{elapsed}, \Delta t_{step}, N_{step}, \Delta V_{step}, T) = P_{def}^{Tot}(\Delta t_{elapsed} - N_{step} \Delta t_{step}, N_{step}, T) + \left[1 - \prod_{j=1}^{N_{step}} \left[1 - P_B \left(\Delta t_{step}, \frac{j \Delta V_{step}}{D}, T \right) \right] \right]. \quad (11)$$

In this case we identify $t_{en} = \Delta t_{elapsed} - N_{step} \Delta t_{step}$ and solving for t_{en} find

$$t_{en}^{Tot}(\Delta t_{step}, N_{step}, \Delta V_{step}, T) = \left(\frac{h}{2k_B T} \right) \left[\sum_{i=A,B} \exp \left[\frac{-\Delta G_{def}^i}{k_B T} \right] \sinh \left[\frac{\epsilon_0 \epsilon_r N_{step}^2}{2k_B T N_{def}^i} \right] \right]^{-1} \times \left\{ \prod_{j=1}^{N_{step}} \left[1 - \left(\frac{2k_B T}{h \Delta t_{step}} \right) \exp \left[\frac{-\Delta G_{def}^B}{k_B T} \right] \sinh \left[\frac{\epsilon_0 \epsilon_r (j \Delta V_{step})^2}{2k_B T N_{def}^B} \right] \right] \right\}. \quad (12)$$

Equation (12) yields the corrected green curve in the inset of Fig. 6.

C. Ramp Rate Dependence

A closely related question is how measured breakdown depends on the ramp rate up to a given voltage. Step-up tests were conducted on Kapton E samples. Ramp rate dependence was investigated by varying the rate of incremental voltage steps to reach electrostatic breakdown. Figure 8 shows slower ramp rates (as low as 20 V steps at 3.5 sec intervals) resulted in >35% lower F_{ESD} values than tests conducted at the maximum ramp rate of 500 V/s recommended in ASTM standards [5].

This effect can be estimated by assuming that only the applied field during the final step-up contributed to the breakdown (equivalent to the yellow curve of Fig. 6), setting the ratio of Eq. (3) evaluated at $\Delta t = 1$ s and $\Delta t = \Delta t_{step}$ equal to the ratio of the experimental ramp rate r to r_0 , and using the relation $\operatorname{arcsinh}(x) = \ln(x + \sqrt{1 + x^2})$. The ramp dependent electric field strength is

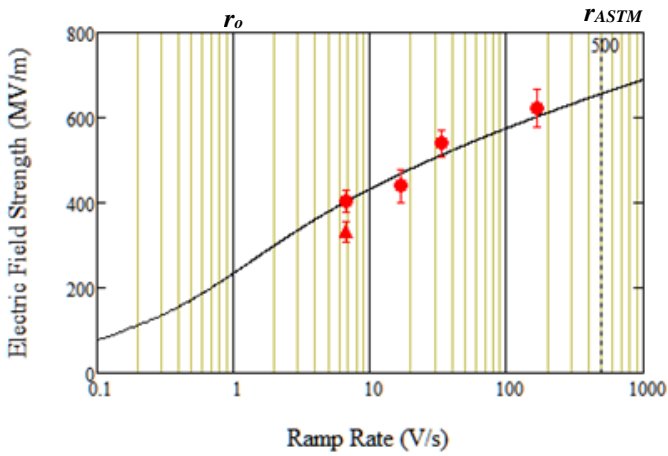


Fig. 8. Electric field strength as a function of ramp rate. Data are shown for 27 μm (circles) and 51 μm (triangle) thick Kapton E samples. Fit is based on Eq. (13), with $r_o=1$ V/s and $F_{ESD}(r_o)=239$ MV/m. The ASTM recommended maximum rate of 500 V/s is indicated [5].

$$F_{ESD}(r) = F_{ESD}(r_o) \cdot \left\{ \ln \left[\frac{r}{r_o} \left(1 + \sqrt{1 + \left(\frac{r_o}{r} \right)^2} \right) \right] \right\}^{1/2}. \quad (13)$$

$F_{ESD}(r_o)$ is the breakdown field strength at $r_o=1$ V/s. The fit to the data in Fig. 8 is very good, using Eq. (13) with $F_{ESD}(r_o)=239$ MeV or equivalently $F_{ESD}(5.7$ V/s)= 373 MV/m at 20 V per 3.5 s.

At slower ramp rates the first approximation breaks down (see Fig. 7). Properly accounting for the probability of breakdown during the step-up time produces a finite asymptotic limiting field as the ramp rate becomes very small, rather than approaching zero field as predicted by Eq. (13).

D. Statistical Analysis of Breakdown Field Strength

The literature and the theoretical discussions above suggest that ESD is a stochastic process [13,15,20,30,40]. Fig. 9 shows the percent of samples broken down versus breakdown field during 89 LDPE and 36 Kapton step-up tests (see Section III). The step-up data are fit (black solid curves) with the two-parameter Weibull distribution for the probability of failure [29,39,40]:

$$P_{def}^W(F) = 1 - \exp \left[- \left(F / F_{def}^W \right)^\beta \right]. \quad (14)$$

The Weibull scale parameter, F_{def}^W , defined as the field corresponding to a 63.2% breakdown cumulative probability, approximates the field associated with the defect energy involved in breakdown. β is the Weibull shape parameter.

For LDPE $\beta=6.96$, in agreement with results Chauvet and Laurent for similar materials of $\beta=6.6$ [40]. For Fig. 9(a), $F_{def}^W=293$ MV/m; comparison of F_{def}^W is difficult due to ~ 10 times faster ramp rate and 10 times thicker samples for the Chauvet and Laurent study [40,41]. For Kapton $\beta=10.9$, in rough agreement with a range of $8 \lesssim \beta \lesssim 22$ for similar polyimide films [42]. For Fig. 9(b), $F_{def}^W=336$ MV/m.

Based on the probabilistic interpretation of the Weibull distribution, we define the onset of breakdowns, F_{onset} as $P_{def}^W(F_{onset}) \equiv 0.0455$ or 2σ below F_{def}^W . Likewise we define the field by which we expect most breakdowns to occur, F_{ESD}

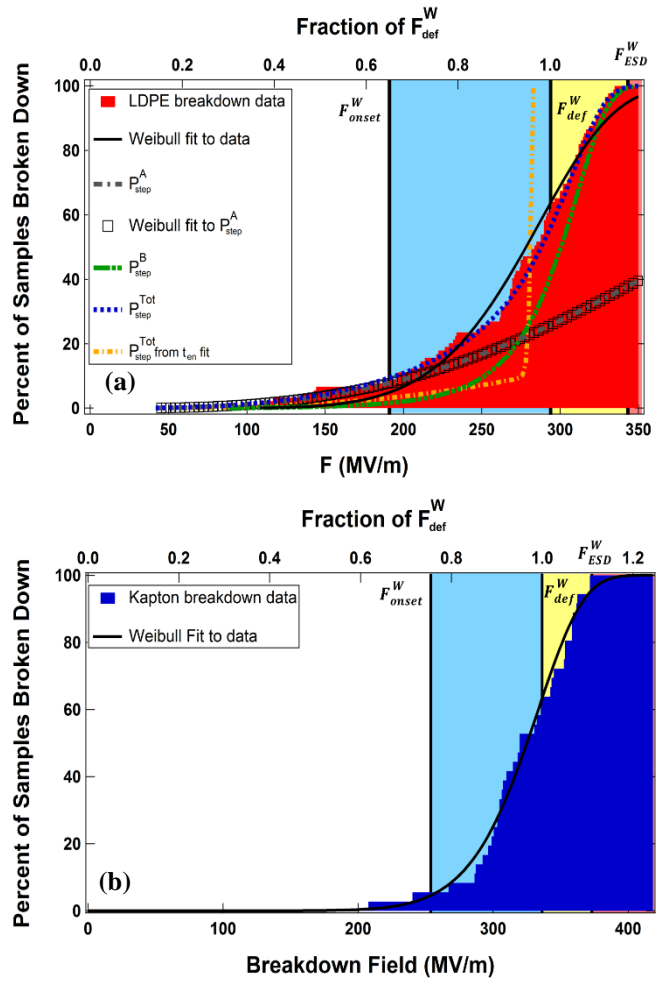


Fig. 9. Histogram of the cumulative fraction of total breakdowns versus breakdown electric field and fraction of F_{def}^W for: (a) LDPE and (b) Kapton. Both data sets were fit to Eq. (14) for the two-parameter Weibull distribution. F_{onset}^W is defined as the field where the fit predicts 5% probability of breakdown and F_{ESD}^W as the field with 95% probability of breakdown. The blue region is the region between F_{onset}^W and F_{def}^W , the yellow region is between F_{def}^W and F_{ESD}^W , and above F_{ESD}^W is the red region.

as $P_{def}^W(F_{ESD}) \equiv 0.9545$ or 2σ above F_{def}^W . In Figs. 6 and 9 F_{onset} to F_{def}^W defines the blue region, F_{def}^W to F_{ESD} defines the yellow region and fields above F_{ESD} are colored in red. For LDPE $F_{onset}^W=189$ MV/m and $F_{ESD}^W=345$ MV/m. For Kapton $F_{onset}^W=253$ MV/m and $F_{ESD}^W=373$ MV/m.

Closer inspection of the Weibull fits to Figs. 9(a) and 9(b) show a consistent discrepancy, with the fit mostly over predicting the breakdown below F_{def}^W and largely under predicting the breakdown above F_{def}^W . The low field data for LDPE in Fig. 9(a) are fit well with one Weibull distribution and the high field data are fit well by a second Weibull distribution. Similar evidence for low- and high-field Weibull distributions have been noted for polyimide [42] and polypropylene [43] films, as discussed in [17].

The dual-mechanism nature of the polymers is modeled by Eq. (10), which can also be used to fit the data in Fig. 9. The orange dot-dashed curve in Fig 9(a) is P_{step}^{Tot} from Eq. (10) using values of ΔG_{def}^A , N_{def}^A , ΔG_{def}^B , and N_{def}^B from our fit to SVET data (Fig. 6). Although this fit exhibits the approximate shape of the distribution, it is not a good fit to the data. A fit to LDPE step up data using Eq. (10) with four adjustable

parameters yields similar values for Type A defects ($\Delta G_{def}^A=0.95$ eV, $N_{def}^A=2.8 \cdot 10^{21}$ cm⁻³), but significantly different values for Type B defects ($\Delta G_{def}^B=1.07$ eV, $N_{def}^B=3.15 \cdot 10^{19}$ cm⁻³). This dual-mechanism fit (blue dotted curve), which is the sum of contributions from Type A defects (black dot-dashed curve) and Type B defects (green dot-dashed curve), is a very good fit to the data. At this point, the discrepancies for the Type B defect parameters, particularly the defect energy, are not understood. This difference could be indicative of another defect mechanism or perhaps results from an approximation in our derivation of Eq. (10), for instance that N_{def}^B is constant. We do note that the crossover field, ≈ 275 MV/m, between P_{step}^A and P_{step}^B (the intersection between the grey and green dashed curves in Fig. 9(a)) is essentially the same as the crossover field for the intersection between t_{en}^A and t_{en}^B (blue and orange dashed curves in Fig. 6).

E. Temperature Dependent Processes

The temperature dependence of F_{ESD} of thin film insulators has been studied with step-up tests conducted over a range of fixed temperatures from $\sim 150 \pm 5$ K to ~ 300 K (see Fig. 10). A small linear temperature dependence of F_{ESD} for LDPE was observed in the range of 150 K to 240 K. There was an abrupt change to a nearly temperature-independent behavior above ~ 240 K. These data are consistent with higher temperature measurements by Shinyama [36] who observed a roughly temperature-independent breakdown field strength of ~ 450 MV/m over 295 K to 330 K at 1kV/s ramp rates for similar 25 μ m thick LDPE samples; F_{ESD} then decreased linearly to ~ 250 MV/m at 385 K. The 1.6X ratio of Shinyama's $F_{ESD} \approx 450$ MV/m at 1kV/s rate with the $F_{ESD} \approx 280$ MV/m at 5.7 V/s in Fig. 10 is consistent with the ratio of 1.8X for similar ramp rates in Fig. 8.

Values for the dominant defect energy and density can be determined from linear fits to the temperature data in Fig. 10. By setting Eq. (3) at breakdown where $P_{def}(\Delta t = t_{en}) = 1$ for two temperatures, $T_1 < T_2$, assuming ΔG_{def} , t_{en} and N_{def} are approximately constant over $T_1 < T < T_2$, and using the approximation $\sinh(x) = x$, we find a temperature-independent ΔG_{def}^T from the slope as

$$\Delta G_{def}^T = \frac{k_B}{(T_1^{-1} - T_2^{-1})} \cdot \ln[F_{def}(T_2)^2 - F_{def}(T_1)^2] \quad (15)$$

and then a temperature dependent N_{def}^T from the value of F_{ESD} at each temperature as

$$N_{def}^T = \frac{\epsilon_0 \epsilon_r}{2} [F_{def}(T)^2 / \Delta G_{def}^T]. \quad (16)$$

For the low temperature branch of Fig. 10 we find $\Delta G_{def}^{LT} = 1.5$ eV and $N_{def}^{155K} = 2.4 \cdot 10^{18}$ cm⁻³ and $N_{def}^{235K} = 5.7 \cdot 10^{18}$ cm⁻³. For the high temperature branch, $\Delta G_{def}^{HT} = 4$ eV and $N_{def}^{240K} \approx N_{def}^{293K} = 1 \cdot 10^{18}$ cm⁻³; the values for these parameters at

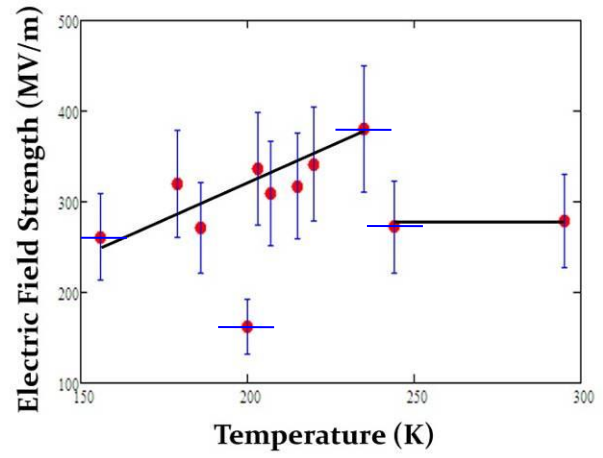


Figure 10. Plot of average breakdown field versus temperature, with separate linear fits below the glass transition temperature at $\sim 240 \pm 10$ K and above it.

high temperature are consistent with room temperature values estimated from other methods in this study.

The observed transition in electric field strength in LDPE may be related to a LDPE structural phase transition observed at between 250 K and 262 K. This β transition is routinely observed in branched polyethylene, and has been associated with conformational changes along polymer chains in the interfacial matrix of disordered polymers between nanocrystalline regions in the bulk. Similar abrupt (often discontinuous) changes near ~ 250 K have been seen in prior studies of mechanical and thermodynamic properties and electron transport properties including dark current conductivity [23,38], radiation induced conductivity [23,44,45], loss tangent [32] and dielectric constant [32]. These changes may result from a discontinuous change in the activation volume at the glass transition to allow a smaller field value to bring about complete breakdown.

VI. FUTURE WORK

To extend the tests of the ESD models, additional time endurance tests will be conducted to improve statistics, to extend to lower fields and longer endurance times, and to test higher fields and shorter t_{en} with more rapid ramp rates up the ASTM suggested maximum rate of 500 V/s. Future research will expand the temperature range of data in Fig. 10 below 120 K and above 300 K towards the polymer melting temperature. Additional tests will be conducted that cool to < 150 K, apply a range of static voltages, and then measure current versus time data as the LDPE warms; these will study synergistic T and t_{en} effects and allow us to more fully understand the processes occurring around the glass transition temperature at ~ 250 K. Better statistics will also be acquired for the statistical analysis of recoverable breakdown events such as those shown in Figs. 6 and 9. Ultimately, different insulating polymers and ceramics (*e.g.*, polyimide, PTFE, SiO₂, and Al₂O₃), with different defect density distributions will be studied.

TABLE I. COMPARISON OF CRITICAL FIELDS, DEFECT ENERGIES AND DEFECT DENSITIES

| Method | LDPE | | Kapton | |
|---|---|--|--|---|
| | Type B Defects | Type A Defects | Type B Defects | Type A Defects |
| Estimation from independent materials properties (Section IV.C) | $F_{def}^{bb} \sim 295$ MV/m $\Delta G_{def}^{bb} = 3.65$ eV/bond $N_{def}^{bb} \approx 1.5 \cdot 10^{18}$ broken bonds/cm ³ | $F_{def}^K \sim 6575$ MV/m $\Delta G_{def}^K = 0.90$ eV $N_{def}^K < 3 \cdot 10^{21}$ Kuhn pairs/cm ³ | $\Delta G_{def}^{bb} = 3.65$ eV/bond. | $F_{def}^K \sim 3226$ MV/m $\Delta G_{def}^K = 1.3$ eV $N_{def}^K < 5 \cdot 10^{20}$ Kuhn pairs/cm ³ |
| Electrostatic Breakdown (Section V.D) | $F_{def}^B = 735$ MV/m $\Delta G_{def}^B = 1.07$ eV $N_{def}^B = 3.15 \cdot 10^{19}$ cm ⁻³ $F_{onset}^W = 189$ MV/m $F_{def}^W = 293$ MV/m $F_{ESD}^W = 345$ MV/m | $F_{def}^A = 6526$ MV/m $\Delta G_{def}^A = 0.95$ eV $N_{def}^A = 2.8 \cdot 10^{21}$ cm ⁻³ | $F_{onset}^W = 253$ MV/m $F_{def}^W = 336$ MV/m $F_{ESD}^W = 373$ MV/m | NA |
| Endurance time measurements (Section V.A) | $F_{def}^B = 320$ MV/m $\Delta G_{def}^B = 3.65$ eV $N_{def}^B = 1.75 \cdot 10^{18}$ cm ⁻³ | $F_{def}^K \sim 10320$ MV/m $\Delta G_{def}^A = 0.95$ eV $N_{def}^A = 7 \cdot 10^{21}$ cm ⁻³ | NA | NA |
| Ramp rate (Section V.C) | $F_{ESD}(5.7 \text{ V/s}) = 373$ MV/m | NA | NA | NA |
| Temperature measurements (Section V.E) | $F_{def}^{293K} = 253$ MV/m $\Delta G_{def}^{293K} = 4$ eV $N_{def}^{293K} = 1 \cdot 10^{18}$ cm ⁻³ | NA | NA | NA |

Taken together, current and proposed measurements will allow us to conduct a comprehensive study of: (i) the stochastic nature of electrostatic breakdown; (ii) application of common statistical methods for used to describe ESD in materials [1,13] (iii) connections to the rate equations (Eqs. (6)), and (iv) a more complete development of the dual mechanism breakdown model of Eq. (10) outlined in this paper.

VII. CONCLUSION

This study of the breakdown of LDPE and polyimide for high applied fields in a capacitive configuration has produced a more complete picture of the time and temperature dependent breakdown behavior that suggests two separate processes are occurring, with their relative contributions to breakdown dependent on the value of applied field. As a result a new dual mechanism model for the probability of breakdown as a function of applied field, time and temperature, based on clearly identifiable physical parameters, has been developed to predict the ESD probability curves for applied field, endurance time, ramp rate, and temperature. This new model correctly predicts breakdown for a large range of applied fields, predicts the general behavior of the unusual transition observed from one process to the other, and yields material parameters from fits to the data that are consistent with previous studies of LDPE and polyimide. Results for the fits for several different measurements for LDPE and more limited polyimide measurements are listed in Table I.

The results of this study point out important consequences for spacecraft charging and other applications that build up charge or have sub-critical fields applied for long time periods. Measurements made with faster ramp rates over predict the breakdown field applicable for very slow charge accumulation by a factor of two or more. Further, the application of sub-critical fields by a factor of 2 or 3 less than the asymptotic breakdown field at short times still has endurance times far less than many typical long duration space missions. Taken together, these suggest that values of F_{ESD}

from standard handbooks, or cursory measurements that have been used routinely in the past, substantially overestimate the field required for breakdown in common spacecraft applications, which often apply sub-critical fields for very long time periods as charge accumulates.

ACKNOWLEDGEMENT

We gratefully acknowledge contributions to the development of the instrument and test methods by Dan Arnfield, Anthony Thomas, Jeri Brunson, Ryan Hoffmann and Justin Dekany. Matthew Stromo, Dan Arnfield, Anthony Thomas helped with ESD data acquisition.

REFERENCES

- [1] K.L. Bedingfield, R.D. Leach and M.B. Alexander, "Spacecraft System Failures and Anomalies Attributed to the Natural Space Environment." NASA Ref. Pub. 1390, NASA MSFC, 1996.
- [2] J.R. Dennison, "The Dynamic Interplay between Spacecraft Charging, Space Environment Interactions and Evolving Materials," 13th Spacecraft Charging Tech. Conf., (Pasadena, CA, June, 2014).
- [3] ASTM D-5213-12, "Standard Specification for Polymeric Resin Film for Electrical Insulation and Dielectric Applications," (American Society for Testing and Materials, 100 Barr Harbor Drive, West Conshohocken, PA, 2012).
- [4] ASTM D 149-97a, "Standard Test Method for Dielectric Breakdown Voltage and Dielectric Strength of Solid Electrical Insulating Materials at Commercial Power Frequencies," (American Society for Testing and Materials, 100 Barr Harbor Drive, West Conshohocken, PA, 2004).
- [5] ASTM D3755-14, "Standard Test Method for Dielectric Breakdown Voltage and Dielectric Strength of Solid Electrical Insulating Materials Under Direct-Voltage Stress," (American Society for Testing and Materials, 100 Barr Harbor Drive, West Conshohocken, PA, 2014).
- [6] J. Brunson, "Measurement of Charge Decay Time and Resistivity of Spacecraft Insulators Using Charge Storage Method and Application to Theoretical Modeling of Charging Behavior of Insulators," PhD Dissertation, Physics, Utah State University, Logan, UT, 2009.
- [7] "Material Information-Polyethylene Low Density LDPE," Goodfellow, Devon, PA, Jan., 2006.
- [8] H.J. Wintle, "Conduction Processes in Polymers," in Engineering Dielectrics--Volume IIA: Electrical Properties of Solid Insulating Materials: Molecular Structure and Electrical Behavior, American Society for Testing and Materials, R. Bartnikas, Editors, (American Society for Testing and Materials, Philadelphia, PA, 1983).
- [9] A.J. Peacock, *Handbook of Polyethylene*, (Marcel Dekker Inc., Basel,

- NY, USA, 2000).
- [10] "Dupont Kapton HN Polyimide Film," Dupont Technical Bulletin H-38479, GS-96-7, Circleville, OH, 2011.
- [11] J.C. Gillespie, "Measurements of the Temperature Dependence of Radiation Induced Conductivity in Polymeric Dielectrics," MS Thesis Utah State University, Logan, UT, 2013.
- [12] ASTM E1559-09, "Standard Test Method for Contamination Outgassing Characteristics of Spacecraft Materials," (American Society for Testing and Materials, 100 Barr Harbor Drive, West Conshohocken, PA, 2012).
- [12] K.C. Kao, *Dielectric Phenomena in Solids*, First ed., (Elsevier Academic Press, New York, 2004).
- [14] T.J. Lewis, "Polyethylene under Electrical Stress," IEEE Trans. Dielectrics and Electrical Insulation, vol. 9, no. 5, pp. 13p, 2002.
- [15] J.P. Crine, "On the interpretation of some electrical aging and relaxation phenomena in solid dielectrics," IEEE Trans. Dielectrics and Electrical Insulation, vol. 12, no. 6, pp. 1089-1107, 2005.
- [16] G.C. Montanari, C. Laurent, G. Teyssedre, *et al.*, "From LDPE to XLPE: investigating the change of electrical properties. Part I. space charge, conduction and lifetime," IEEE Trans. Dielectrics and Electrical Insulation, vol. 12, no. 3, pp. 438-446, 2005.
- [17] L.A. Dissado and J.C. Fothergill, *Degradation and Breakdown in Polymers*, IEE Materials and Devices Series 9, G.C.Stevens, Ed., (Peter Peregrinus, London, 1992).
- [18] J.C. Anderson, K.D. Leaver, P. Leever and R.D., Rawlings, *Materials Science for Engineers*, 5th Ed. (Nelson Thornes, Ltd., Cheltenham, UK, 1990).
- [19] J.P. Crine, J.L. Parpal, and C. Dang, "A new approach to the electric aging of dielectrics," IEEE Conf. on Electrical Insulation and Dielectric Phenomena, Annual Report, pp. 161-167, Nov. 1989.
- [20] J.-L. Parpal, J.-P. Crine, and C. Dang, "Electrical aging of extruded dielectric cables. A physical model," IEEE Trans. Dielectrics and Electrical Insulation, vol. 4, no. 2, pp. 197-209, 1997.
- [21] C. Dang, J.-L. Parpal, J.P. Crine, "Electrical Aging of Extruded Dielectric Cables: Review of Existing Theory and Data," IEEE Trans. Dielectrics and Insulators, Vol. 3, No. 2, April 1996, 237-247.
- [22] N.F. Mott and E.A. Davis, *Electronic Processes in Non-Crystalline Materials*, 2nd Ed. (Oxford University Press, Oxford, 1979).
- [23] J.R. Dennison, A. Sim, J. Brunson, S. Hart, J. Gillespie, J. Dekany, C. Sim and D. Arnfield, "Engineering Tool for Temperature, Electric Field and Dose Rate Dependence of High Resistivity Spacecraft Materials Paper Number," AIAA-2009-0562, Proceedings of the 47th American Institute of Aeronautics and Astronautics Meeting on Aerospace Sciences, 2009.
- [24] A. Miller and E. Abrahams, "Impurity Conduction at Low Concentrations," Phys. Rev., vol. 120, 745, 1960.
- [25] T.J. Lewis, "Charge transport, charge injection and breakdown in polymeric insulators," J. Phys. D: Applied Phys., vol. 23, no. 12, pp. 1469, 1990.
- [26] A.M. Sim and J.R. Dennison, "Comprehensive Theoretical Framework for Modeling Diverse Electron Transport Experiments in Parallel Plate Geometries," Paper Number, AIAA-2013-2827, 5th AIAA Atmospheric and Space Environ. Conf., (San Diego, CA, June, 2013).
- [27] P. Trnka, M. Sirucek, M. Svoboda, *et al.*, "Condition-based maintenance of high-voltage machines-a practical application to electrical insulation," IEEE Electrical Insulation Magazine, vol. 30, no. 1, pp. 32-38, 2014.
- [28] T. Czaszejko, "High-voltage testing fundamentals: a cable testing perspective," IEEE Electrical Insulation Magazine, vol. 30, no. 1, pp. 7-13, 2014.
- [29] C.L. Griffiths, J. Freestone, R.N. Hampton, "Thermoelectric Aging of Cable Grade XLPE," Conf. Record of IEEE Intern. Symp. Electrical Insulation, Arlington, VA, 1998, pp. 578-582.
- [30] T.J. Lewis, J.P. Llewellyn, M.J. van der Sluijs, *et al.*, "A new model for electrical ageing and breakdown in dielectrics," IEE Conf. Pub., vol. 430, Dielectric Materials, Measurements and Applications, pp. 220-224, 1996.
- [31] J.P. Crine, "On the interpretation of some electrical aging and relaxation phenomena in solid dielectrics," IEEE Trans. Dielectrics and Electrical Insulation, vol.:12, no. 6, pp. 1-16, Dec. 2005.
- [32] P.J. Phillips, "Morphology and Molecular Structure of Polymers and Their Dielectric Behavior," in Engineering Dielectrics - Volume IIA: Electrical Properties of Solid Insulating Materials: Molecular Structure and Electrical Behavior, American Society for Testing and Materials, R. Bartnikas, Editors, (American Society for Testing and Materials, Philadelphia, PA 19103, 1983).
- [33] A.R. Fredrickson, and J.R. Dennison, "Measurement of conductivity and charge storage in insulators related to spacecraft charging," IEEE Trans. Nucl. Sci. Vol. 50, No. 6, 2003, pp. 2284-2291.
- [34] R. Hoffmann, J.R. Dennison, J. Albreten, "Flux and Fluence Dependence of Electron Emission for High-yield, High-resistivity Materials: Implications for Spacecraft Charging," Proc.47th Am. Institute of Aeronautics and Astronautics Meeting on Aerospace Sciences. 2009, pp. AIAA-2009-0348.
- [35] L. Torrisi, N. Campo, L. Auditore, R. Barnà, D. De Pasquale, A. Italiano, A. Trifirò, M. Trimarchi and G. Di Marco, "Mechanical modifications in dense polyethylene induced by energetic electron beams, Radiation Effects and Defects in Solids: Incorporating Plasma Science and Plasma Technology, (2004) 159:11-12, 597-606, 2004.
- [36] K. Shinyama, S. Fujita, "Mechanical and Dielectric Breakdown Properties of Eco-friendly Dielectric Materials," Int. J. Soc. Mater. Eng. Resour. 13, 2,2006.
- [37] R. Zallen, *The Physics of Amorphous Solids*, New York: Wiley, 1983.
- [38] J.R. Dennison and J. Brunson, "Temperature and Electric Field Dependence of Conduction in Low-Density Polyethylene," IEEE Trans. Plasma Sci., 36(5), 2246-2252, 2008.
- [39] H. Cho, Y.C. Kim, S.O. Kim and I.J. Chung, "Persistence length calculation from light scattering and intrinsic viscosity of dilute semiflexible polyimide solutions with different degree of imidization," Korea-Australia Rheology Journal, vol. 12, no. 1, pp. 69-76, 2000
- [40] C. Chauvet and C. Laurent, "Weibull Statistics in Short-term Dielectric Breakdown of Thin Polyethylene Films," IEEE-Trans. Elec. Insulation, vol. 28, no. 1, p. 18, 1993.
- [41] Y. Sekii, K. Asakawa and K. Mouri, "Statistical Investigation of Dielectric Breakdown of LDPE," Proc. 2001 Intern. Symp. on Electrical Insulating Materials (ISEIM 2001), pp. 562-565, Nov., 2001.
- [42] S. Diahm, S. Zelmat, M.-L. Locatelli, S. Dinculescu, M. Decup and T. Lebey, "Dielectric Breakdown of Polyimide Films: Area, Thickness and Temperature Dependence," IEEE-Trans. Dielectrics and Electrical Insulation, vol. 17, no. 1; pp. 18-27, 2010
- [43] J. S. J. Laihonon, U. Gäfvert, T. Schütte, and U. W. Gedde, "DC Breakdown Strength of Polypropylene Films: Area Dependence and Statistical Behavior", IEEE Trans. Dielectr. Electr. Insul., Vol. 14, pp. 275-286, 2007.
- [44] J.R. Dennison, J. Gillespie, J.L. Hodges, R.C. Hoffmann, J. Abbott, A.W. Hunt and R. Spalding, "Radiation Induced Conductivity of Highly-Insulating Spacecraft Materials," in Application of Accelerators in Research and Industry, Am. Instit. Phys. Conf. Proc. Series, Vol. 1099, ed. F.D. McDaniel and B. L. Doyle, (Am. Instit. of Phys., Melville, NY, 2009), pp. 203-208.
- [45] J.C. Gillespie, J.R. Dennison, and A.M. Sim, "Density of State Models and Temperature Dependence of Radiation Induced Conductivity," Proc. 13th Spacecraft Charging Techn. Conf., (Pasadena, CA, June, 2014).



Allen Andersen is currently a graduate student at Utah State University in Logan, UT pursuing a PhD in physics. He received a BS degree in physics from BYU-Idaho in 2012. He has worked with the Materials Physics Group for two years on electron transport measurements, electrostatic discharge tests, and electron emission measurements related to spacecraft charging.



JR Dennison received the B.S. degree in physics from Appalachian State University, Boone, NC, in 1980, and the M.S. and Ph.D. degrees in physics from Virginia Tech, Blacksburg, in 1983 and 1985, respectively. He was a Research Associate with the University of Missouri—Columbia before moving to Utah State University (USU), Logan, in 1988. He is currently a Professor of physics at USU, where he leads the Materials Physics Group. He has worked in the area of electron scattering for his entire career and has focused on the electron emission and conductivity of materials related to spacecraft charging for the last two decades.



Alec Sim received a BS degree in physics from the University of California-San Bernardino, CA in 2004, an MS in physics from the University of Kentucky in Lexington, KY in 2008, and a PhD from Utah State University in Logan, UT in 2013. He worked with the Materials Physics Group for six years on electron emission measurements and theoretical studies of electron transport in highly disordered insulating materials. He is currently an Assistant Professor in the Department of Physical Sciences at Irvine Valley College, Irving CA.



Charles Sim received a BS in physics from Utah State University, Logan, UT in 2013. He worked with the Materials Physics Group for three years on tests of electrostatic breakdown and conductivity in highly insulating disordered materials. He is currently a technician at CR Bard.